Materials Today Bio 13 (2022) 100182

Contents lists available at ScienceDirect

Materials Today Bio

journal homepage: www.journals.elsevier.com/materials-today-bio

Investigation of the role of the autophagic protein LC3B in the regulation of human airway epithelium cell differentiation in COPD using a biomimetic model

Shiue-Luen Chen [a,b], Hsiao-Chun Chou [b], Kuan-Chen Lin [b,c], Jia-Wei Yang [a,b], Ren-Hao Xie [a,b], Chong-You Chen [a,b], Xin-Yi Liu [b], Johnson H.Y. Chung [d], Guan-Yu Chen [a,b,e,*]

[a] Department of Electrical and Computer Engineering, College of Electrical and Computer Engineering, National Yang Ming Chiao Tung University, Hsinchu, Taiwan
[b] Institute of Biomedical Engineering, College of Electrical and Computer Engineering, National Yang Ming Chiao Tung University, Hsinchu, Taiwan
[c] Division of Haematology/Oncology, Department of Internal Medicine, Chang Gung Memorial Hospital (Linkou), Taoyuan, Taiwan
[d] ARC Centre of Excellence for Electromaterials Science, Intelligent Polymer Research Institute, University of Wollongong, Wollongong, NSW, Australia
[e] Department of Biological Science and Technology, National Yang Ming Chiao Tung University, Hsinchu, Taiwan

ARTICLE INFO

Keywords:
Chronic obstructive pulmonary disease
Airway epithelial cells
Autophagy
Cell differentiation
Cilia beating

ABSTRACT

Chronic obstructive pulmonary disease (COPD) is one of the most lethal chronic disease worldwide; however, the establishment of reliable *in vitro* models for exploring the biological mechanisms of COPD remains challenging. Here, we determined the differences in the expression and characteristics of the autophagic protein LC3B in normal and COPD human small airway epithelial cells and found that the nucleus of COPD cells obviously accumulated LC3B. We next established 3D human small airway tissues with distinct disease characteristics by regulating the biological microenvironment, extracellular matrix, and air-liquid interface culture methods. Using this biomimetic model, we found that LC3B affects the differentiation of COPD cells into basal, secretory, mucous, and ciliated cells. Moreover, although chloroquine and ivermectin effectively inhibited the expression of LC3B in the nucleus, chloroquine specifically maintained the performance of LC3B in cytoplasm, thereby contributing to the differentiation of ciliated cells and subsequent improvement in the beating functions of the cilia, whereas ivermectin only facilitated differentiation of goblet cells. We demonstrated that the autophagic mechanism of LC3B in the nucleus is one factor regulating the ciliary differentiation and function of COPD cells. Our innovative model can be used to further analyze the physiological mechanisms in the *in vitro* airway environment.

1. Introduction

Chronic obstructive pulmonary disease (COPD), a common respiratory condition characterized by partly reversible airflow limitation, is predicted to become one of the major causes of disability and death in the next decade worldwide [1–3]. However, the mechanisms driving the induction of chronic inflammation, emphysema, and altered lung function are unclear. Although various biomimetic models of COPD exist and are used to emulate lung inflammation and drug responses [4–6], more reliable *in vitro* models are urgently needed to explore the potential biological mechanisms.

Autophagy is a catabolic process that is essential for maintaining homeostasis under physiological and pathological conditions. When the autophagic response is unregulated, reactive oxygen species production is increased, playing a role in COPD onset [7]. In addition, stimulating the airway epithelial cells of COPD with interleukin-13 can cause functional damage, such as mucous cell proliferation, reduced cilia length, and reduced beating frequency and is related to increased expression of the autophagic proteins LC3B and p62 [8,9]. Specifically, LC3B is highly expressed in cilia cells, whereas its expression is lower in basal and goblet cells. Thus, in COPD, autophagy regulates the differentiation mechanism of airway epithelial cells, and LC3B is a key regulator of cilia cell functions [10,11].

LC3B can be used as a marker for autophagosomes. Accordingly, its co-localization with lysosomes in the cytoplasm is used to assess the degree of autophagy [12]. However, recent evidence has revealed that

* Corresponding author. Institute of Biomedical Engineering, College of Electrical and Computer Engineering, National Yang Ming Chiao Tung University, Hsinchu, Taiwan.
E-mail address: guanyu@nctu.edu.tw (G.-Y. Chen).

https://doi.org/10.1016/j.mtbio.2021.100182
Received 10 November 2021; Accepted 2 December 2021
Available online 8 December 2021

LC3B is also expressed in the nucleus, and its translocation of the nucleus affects cell differentiation [13,14]. Chloroquine (CQ) can prevent the binding of autophagosomes and lysosomes by altering the acidic environment of lysosomes [15,16]; thus, it shows potential for regulating the expression of LC3B in the cytoplasm and nucleus. Ivermectin (IVM), an antiparasitic drug approved by the United States Food and Drug Administration, specifically inhibits importin α/β-mediated nuclear import and can prevent the accumulation of LC3B in the nucleus during autophagy [17,18]. Although the mechanisms related to CQ, IVM, and COPD are unclear, regulation of the autophagic response or LC3B shows considerable potential for regulating the differentiation of COPD cells.

Here, we observed a significant difference in LC3B expression between the nuclei of normal and COPD cells. We subsequently established a biomimetic airway differentiation model and compared the differentiation of basal, club, goblet, and ciliated cells. To evaluate the mechanism of regulation and cell differentiation, we further clarified the effects of CQ and IVM stimulation on the differentiation of human small airway epithelial cells (HSAECs) in cilia and mucus. Our biomimetic *in vitro* model was used to reveal the biological mechanisms regulating the differentiation of HSAECs.

2. Methods

2.1. Cell culture

Normal human HSAECs (PCS-301-010) and COPD HSAECs (PCS-301-013) were purchased from ATCC (Manassas, VA, USA). The bronchial epithelial cell growth kit (PCS-300-040, ATCC) was expanded according to the manufacturer's protocol at 37 °C in a 5% CO_2 incubator.

2.2. Stimulants and inhibitors

HSAECs of normal and COPD were stimulated with 50 μg/mL lipopolysaccharide (LPS; L2630, Sigma, St. Louis, MO, USA) for 24 h after seeding into well-plate. Autophagy inhibitors were screened with a high-content imaging system. The experimental concentrations for analyzing the subsequent autophagy reaction, LC3B expression in the nucleus and cytoplasm, and small airway cell differentiation were 10 μM for CQ (1825–100, Biovision, Milpitas, CA, USA), 200 μM for IVM (I8898, Sigma), and 200 μM for 3-methyladenine (3-MA, tlrl-3ma, InvivoGen, San Diego, CA, USA).

2.3. Cell viability and apoptosis

HSAECs were cultured and treated with or without CQ, IVM, or 3-MA for 48 h after seeding into well-plate. The cells were stained with a CellCheck™ Viability/Cytotoxicity kit (A017, BioScience) or CellEvent™ Caspase-3/7 Green Detection Reagent (C10723, Invitrogen, Carlsbad, CA, USA). After washing, the cells were analyzed with a high-content imaging system.

2.4. Observation of LC3B expression and live cell imaging of the autophagic response

To observe LC3B, normal and COPD cells were cultured in a 24-well plate (9500 cells/well) and treated with or without LPS, CQ, IVM, or 3-MA for 48 h. After washing with phosphate-buffered saline (PBS), the cells were fixed and permeabilized as described previously [19], washed again with PBS, and incubated with a primary antibody specific for LC3B for 1 h at 25 °C. After washing with PBS, the cells were incubated with the secondary antibody for 1 h at room temperature in the dark. The cells were washed and then counterstained with 4,6-diamidino-2-phenylindole (DAPI, Vector Labs, Burlingame, CA, USA) and imaged with a high-content imaging system and confocal microscope. For live cell imaging of autophagy, the cells treated with or without CQ, IVM, and 3-MA were stained with 0.1 μM DAP Green-Autophagy Detection (D676, Dojindo, Kumamoto, Japan) at 0, 2, 4, 6, 8, and 10 h after drug treatment; the cells were incubated at 37 °C in 5% CO_2 in the high-content imaging system for fluorescence imaging and analysis.

2.5. Total protein preparation and western blot analyses

Normal and COPD cells were cultured in a 6-well plate (45,000 cells/well) and treated with or without CQ or IVM for 48 h. The cells were trypsinized and neutralized, followed by centrifugation (500×*g*, 5 min, room temperature). The cell pellets were collected and lysed in 1X RIPA lysis buffer (ab15603, Abcam, Cambridge, UK) supplemented with EDTA-free Protease Inhibitor Cocktail (40693159001, Sigma-Aldrich). Protein concentrations were determined using a Pierce™ BCA Protein Assay Kit (23225, Thermo Fisher Scientific, Waltham, MA, USA) according to the manufacturer's instructions. Cell lysate supernatants were mixed with 4X loading dye and separated by SDS-PAGE. After electrophoresis, proteins were transferred to polyvinylidene fluoride membranes. PBS containing Tween 20 and 5% (w/v) non-fat milk were applied for membranes blocking. Next, the membranes were stained with primary antibodies, after which secondary antibodies were applied to detect primary antibodies. Information on the antibodies used in western blot analyses is shown in Supplementary Table S1. Proteins were analyzed with Immobilon Western Chemiluminescent HRP Substrate (WBKLS0500; Merck Millipore, Billerica, MA, USA) using an Amersham™ Imager 600 system (GE Healthcare, Little Chalfont, UK).

2.6. Cell differentiation

For cell differentiation at the air-liquid interface (ALI), 300 μg/mL collagen I (A1048301, Thermo Fisher Scientific) was coated on both sides of the membrane of a 12-mm transwell plate with a pore size of 0.4 μm overnight before cell seeding. HSAECs were first cultured in a PneumaCult Ex-Plus medium (05040, STEMCELL Technologies, Vancouver, Canada). The cells were then submerged in the extracellular matrix-coated transwell plate at a seeding density of 90,000 cells/well for 4–5 days. After the cells reached 80% confluence, the upper layer of the medium was removed, and the lower layer was changed to the differentiation medium PneumaCult ALI (05001, STEMCELL Technologies) for ALI culture for 4–5 weeks. During this period, the medium was changed every three days, and the upper layer was rinsed with Dulbecco's PBS (DPBS) (33919003, Corning, Inc., Corning, NY, USA; without Ca^{2+} and Mg^{2+}) every two weeks to facilitate cell growth. The cells were treated with CQ or 3-MA for 48 h before changing to ALI. IVM was continuously applied from ALI day 3, and the medium was changed every three days.

To improve mucus exclusion, guaiacol glycerol ether (93-14-1, Tokyo Chemical Industry, Tokyo, Japan) and *S*-(carboxymethyl)-L-cysteine (638-23-3, Tokyo Chemical Industry) were combined with IVM during ALI culture. The final concentrations used in mucus treatment were 100 μM of guaiacol glycerol ether or 10 μM of *S*-(carboxymethyl)-L-cysteine in IVM solution. During this period, the medium was changed every three days, and the upper layer was rinsed with DPBS to remove mucus accumulation.

2.7. SEM and cilia observation

After the cells were differentiated, they were rinsed with DPBS. Next, 2.5% glutaraldehyde (G6257, Sigma) was added to PBS to fix the cells at room temperature for 1 h. After removing the fixative, the samples were rinsed three times with DPBS. To dehydrate the cell samples, we used ethanol (32221, Sigma) with a concentration gradient from low to high (35%, 70%, 85%, 95%) at each concentration for 10 min. After reacting the samples with 100% ethanol for 20 min, 100% hexamethyldisilazane (A15139, Alfa Aesar) was applied as a desiccant for 5 min. After the reaction, the hexamethyldisilazane was removed, and the samples were evaporated and dried for 24 h. The samples were observed with a high-resolution thermal field emission scanning electron microscope (JSM-

7610F, JEOL, Tokyo, Japan) to detect the growth and distribution of ciliated cells after differentiation.

2.8. Immunofluorescence staining

The cells were fixed and permeabilized with Cytofix/Cytoperm (554722, BD Biosciences, Franklin Lakes, NJ, USA) at room temperature for 15 min, rinsed with DPBS three times, and blocked with blocking buffer (1% bovine serum albumin/5% fetal bovine serum in DPBS) at room temperature for 1 h. The cells were incubated with primary antibody for 90 min, washed with DPBS, incubated with secondary antibody (see Supplementary Table S2) for 90 min, washed with DPBS, counterstained with DAPI, and visualized with the high-content imaging system and confocal microscopy.

2.9. Cilia beating and particle removal efficiency

Normal and COPD HSAECs were video-recorded for 10 s on day 30, in ALI cultures (Supplementary Fig. 1). Imaging was conducted at 125 frames per second. The format was 14 bits, and the acquisition matrix was 536 × 536. The exposure time was set to 10 ms and the analog signal was increased, which can support the number of image frames above 30 to facilitate observation of the cilia beating frequency without distortion. By slowing the video speed, the average number of cilia beats per second (of more than 10,000 cilia) was calculated, and the average value from three fields-of-view was used for quantitative analyses.

To explore the ability of cilia to remove particles, a 100-μL solution of red fluorescent particles (FluoSpheres™ carboxylate-modified microspheres, 2 μm, red fluorescence (580/605), 2% solids, F8826, Thermo Fisher Scientific) was divided in aliquots of 2 μg/mL and added to the differentiated cells. Video recordings (magnification of 15 ×) were acquired to calculate the movement distance of the particles within a 3-s period to determine the transport velocity and to quantitatively analyze the movement distance of the particles per unit time.

2.10. Quantitative analysis with high-content imaging system

We used the ImageXpress® Micro 4 high-content imaging system (Molecular Devices, Sunnyvale, CA, USA) equipped with built-in MetaXpress® high-content image acquisition and analysis software. Users can perform high-quality image acquisition and analysis, including bright field and fluorescent imaging, on live or fixed cells and use the application modules for more accurate quantitative analysis and detection. Differentiated HSAECs were analyzed using this customized module. Each fluorescent molecule (DAPI, Alexa488, Alexa633) and its corresponding channel (DAPI, fluorescein isothiocyanate, Cy5) were used in the [Setup]. [Find Round Objects] was then used to detect the nuclei, and [Grow Objects Without Touching] was employed to define the nuclear boundaries (DAPI). To quantify the cilia, we used [HDome] to filter out the background light from the cilia image, and then used [Simple Threshold] to identify the required fluorescence intensity range (Alexa488). Subsequently, we used [Filter Mask] to circle the cilia. [Compare images] was used to compare the original image and listed cilia. If the outcome was correct, the [Keep Marked Object] was used to mark the cells with cilia. To quantitatively analyze the mucus, we used [HDome] to filter out the background light. We then used [Simple Threshold] to identify the required fluorescence intensity interval (Cy5), and then used [Fill Holes] to form a fluorescent block for the benefit of [filter mask]. The area with fluorescence was circled, and finally the goblet cells were marked with [Keep Marked Object]. After completion, we used [Measure] to measure the cilia and mucous cells. We exported the results into Excel files for statistical analyses.

2.11. Statistical information

Experiments were performed at least three times, and the data are reported as the means ± standard deviations. Statistical analysis was performed with GraphPad Prism 6 software (GraphPad, Inc., La Jolla, CA, USA) or with Excel (Microsoft, Redmond, WA, USA). Student's *t*-test was used for statistical analysis of unpaired data, and one-way analysis of variance was used for multiple comparisons.

3. Results

3.1. Different LC3B expression in HSAECs of normal and COPD

To explore the physiological mechanisms of COPD *in vitro*, we first compared normal and COPD HSAECs. After culturing these two cell types under the same conditions, there were no obvious differences in cell viability or caspase 3/7 staining (Fig. 1a–c). However, the HSAECs of COPD contained more vacuoles (sizes of ~4–20 μm) (Fig. 1d), which is a morphological feature of autophagy [20]. To clarify the differences in autophagic characteristics, both cells were cultured for 24 h and examined to detect red fluorescence-labeled LC3B. Confocal imaging revealed that the HSAECs of COPD had higher expression of LC3B and a large number of LC3B puncta in the nucleus compared to normal cells (Fig. 1e). To quantitatively analyze the differences between LC3B puncta in these two cells, we used a high-content imaging system that allowed for fine control of the culture environment and high-throughput cell imaging. This was used in conjunction with a customized module built within MetaXpress software for quantitative analyses (Fig. 1f). Using this method, the LC3B puncta and cell nucleus can be accurately identified. These analyses showed that the relative cell number of nuclear LC3B (≥10 puncta) in COPD cells was approximately 3.5-fold higher than that in the normal group (Fig. 1g). Interestingly, when normal cells were stimulated with LPS for 24 h (Fig. 1h–j), the LC3B puncta also increased considerably, whereas COPD cells maintained their original large numbers (Fig. 1k and l), indicating that the expression of LC3B puncta in the nucleus can be regulated by external stimuli. After LPS stimulation of normal cells, the expression in the nucleus was closer to that of COPD cells. These results demonstrate that in addition to the previous findings that 1) COPD has higher autophagic activity [21] and 2) the lung tissue contains a larger number of autophagic vacuoles [22], the localization of LC3B puncta in the nuclei of COPD cells was also higher than that of normal cells, and the regulation of nuclear LC3B levels may further clarify the physiological mechanism and subsequent differentiation strategies of COPD cells.

3.2. Expression regulation of LC3B in the nucleus of COPD cells

To determine the role of LC3B in the nucleus, we used CQ and IVM to inhibit the expression of the LC3B puncta in the COPD cell nucleus (Fig. 2a and b). Live cell imaging of autophagy showed that the autophagic response in COPD cells was significantly stronger than that in normal cells (Fig. 2c). CQ started to inhibit the nuclear autophagy response after 2 h of treatment, with most of the fluorescence signal accumulating in the cytoplasm. Compared with CQ, IVM reduced the response of nuclear autophagy, but the fluorescence signal in the cytoplasm was lower than that after CQ stimulation. Similar results were observed in confocal imaging, with both drugs effectively reducing the expression of LC3B puncta in the nucleus of COPD cells after 24 h of stimulation (Fig. 2d). The expression of LC3B in the cytoplasm after CQ stimulation was indeed higher than that following mock and IVM stimulation (Fig. 2e and f). Concentrations of 10 μM CQ and 200 μM IVM were selected as optimal concentrations that did not significantly affect cell viability (Fig. 2g). These results indicate that although these two

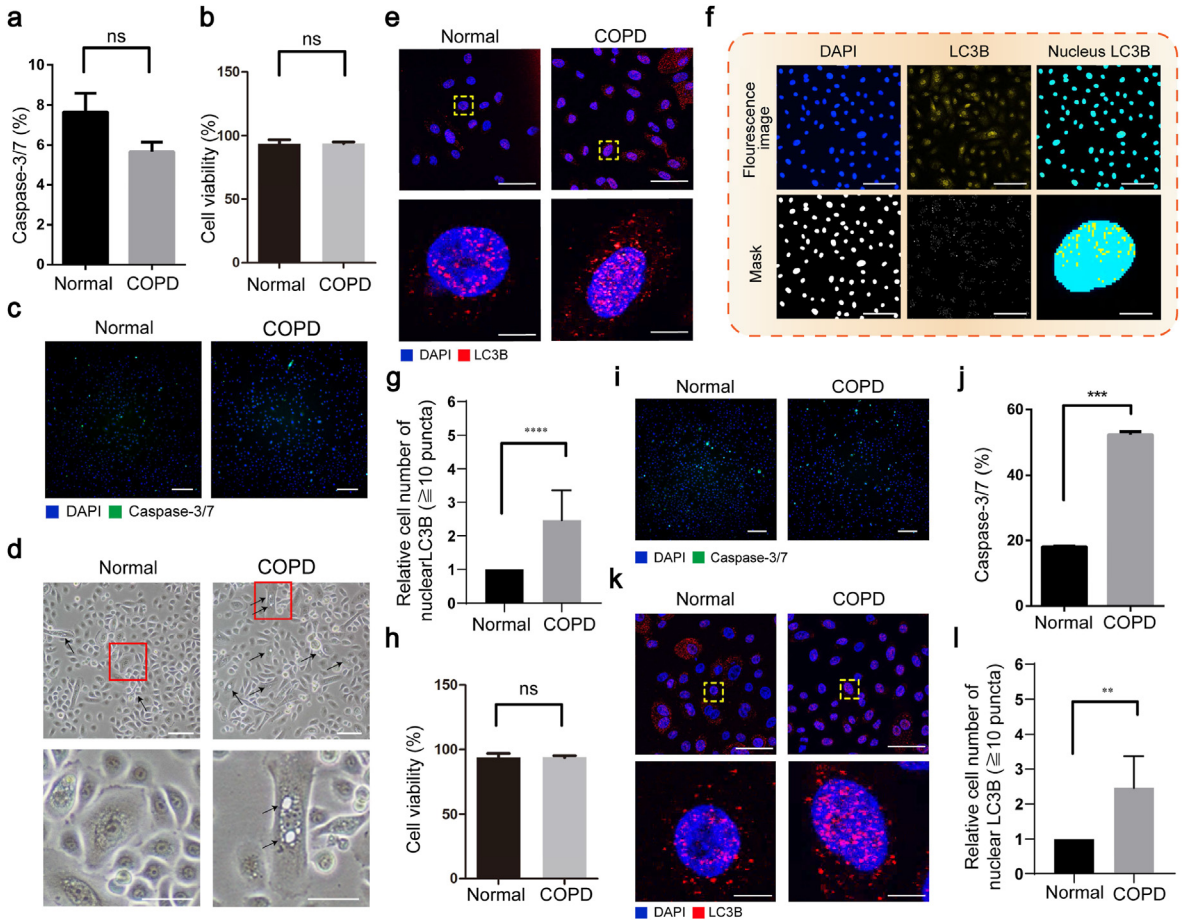

Fig. 1. LC3B expression in normal and COPD HSAECs. a–c) Quantitative analysis of caspase-3/7 and cell viability and high-content imaging of live cells. (c) Cells were stained with DAPI (blue) and caspase-3/7 (green). d) Bright field images showed that vacuoles were produced in COPD cells. e) Confocal image of the difference in LC3B accumulation. Cells were stained with DAPI (blue) and LC3B (red). f) A customized module of MetaXpress software for the high-content imaging system was used to automatically calculate the number of LC3B puncta in the nucleus. The nuclei (blue) and LC3B puncta (yellow) were classified. Top scale bar: 50 μm, right bottom scale bar: 10 μm. g, h) Quantitative analysis of the difference in LC3B puncta in the nucleus and cell viability. i, j) Caspase-3/7 staining and quantitative analysis between normal and COPD groups after 24 h of LPS stimulation. Cells were stained with DAPI (blue) and caspase-3/7 (green). (c), (d), (i) Scale bar: 50 μm. k, l) Changes in LC3B puncta in the nucleus after LPS stimulation according to confocal image and quantitative analysis. Cells were stained with DAPI (blue) and LC3B (red). (e), (k) Top scale bar: 50 μm, bottom scale bar: 10 μm. ns: not significant. *P < 0.05, **P < 0.01, ***P < 0.001; values represent the mean ± SEM values. Each group was evaluated in 3 independent experiments, with 4–6 transwells in each group. Three fields were selected in each transwell, and each field was evaluated with the high-content imaging system to image more than 1000 cells in a single experiment. (For interpretation of the references to colour in this figure legend, the reader is referred to the Web version of this article.)

inhibitors regulate different signaling pathways, they both inhibit the expression of LC3B puncta in the nucleus (Fig. 2h) but differ is their expression and distribution in the cytoplasm.

3.3. *Establishment of an in vitro biomimetic differentiation model of small airways*

To effectively reconstruct the *in vitro* human small airway model, we first compared the ALI culture and general submerged culture method. The ALI-cultured HSAECs were more compact after differentiation (Supplementary Fig. 2a and b) and showed poorly expressed epithelial tight junctions following staining of ZO-1 protein (Supplementary Fig. 2c–e), which has previously been shown to be related to the degree of cell differentiation [23]. These findings demonstrate that ALI culture is necessary for HSAEC differentiation. Therefore, to establish the biomimetic model of small airways, the HSAEC differentiation method involved a) submerging cells in media until they became ~80% confluent and b) changing the culture environment to the ALI to closely emulate the physiological microenvironment (Fig. 3a). When normal and COPD cells were subjected to ALI differentiation for 30 days, the bonds between COPD cells were weakened and led an obvious reduced functionality in the tight junction (Fig. 3b). Subsequently, we observed the growth density and morphology of the cilia differentiated from COPD cells using scanning electron microscopy (SEM) (Fig. 3c). Based on quantitative analyses, the expression of ZO-1 of COPD cells was 14% lower than in normal cells and the cilia lengths were shortened by nearly 45% (Fig. 3d and e). Thus, the efficiency of excluding particles and pathogens by motile cilia may also be greatly reduced.

Subsequently, we used a high-content imaging system and confocal imaging to analyze four types of differentiated cells, including basal, club, goblet, and ciliated cells, and observed significant differences between the normal and COPD groups (Fig. 3f). Basal cells can be defined as progenitor cells with the ability to differentiate into the other three types [24]. The quantitative results showed that the proportion of basal cells in the normal group was similar (within 5–10%) to the actual proportion in humans (Supplementary Table S3), whereas the proportion in the COPD group was as high as 15% (Fig. 3g). This may be because COPD cells exhibit poor cell differentiation. Thus, there were more basal cells remaining in the initial basal form that were unable to differentiate into functional cilia and mucus [25,26]. Club cells can regulate lung stability and participate in immune responses related to airway inflammation [27]. The numbers of club cells and ciliated cells after COPD cell

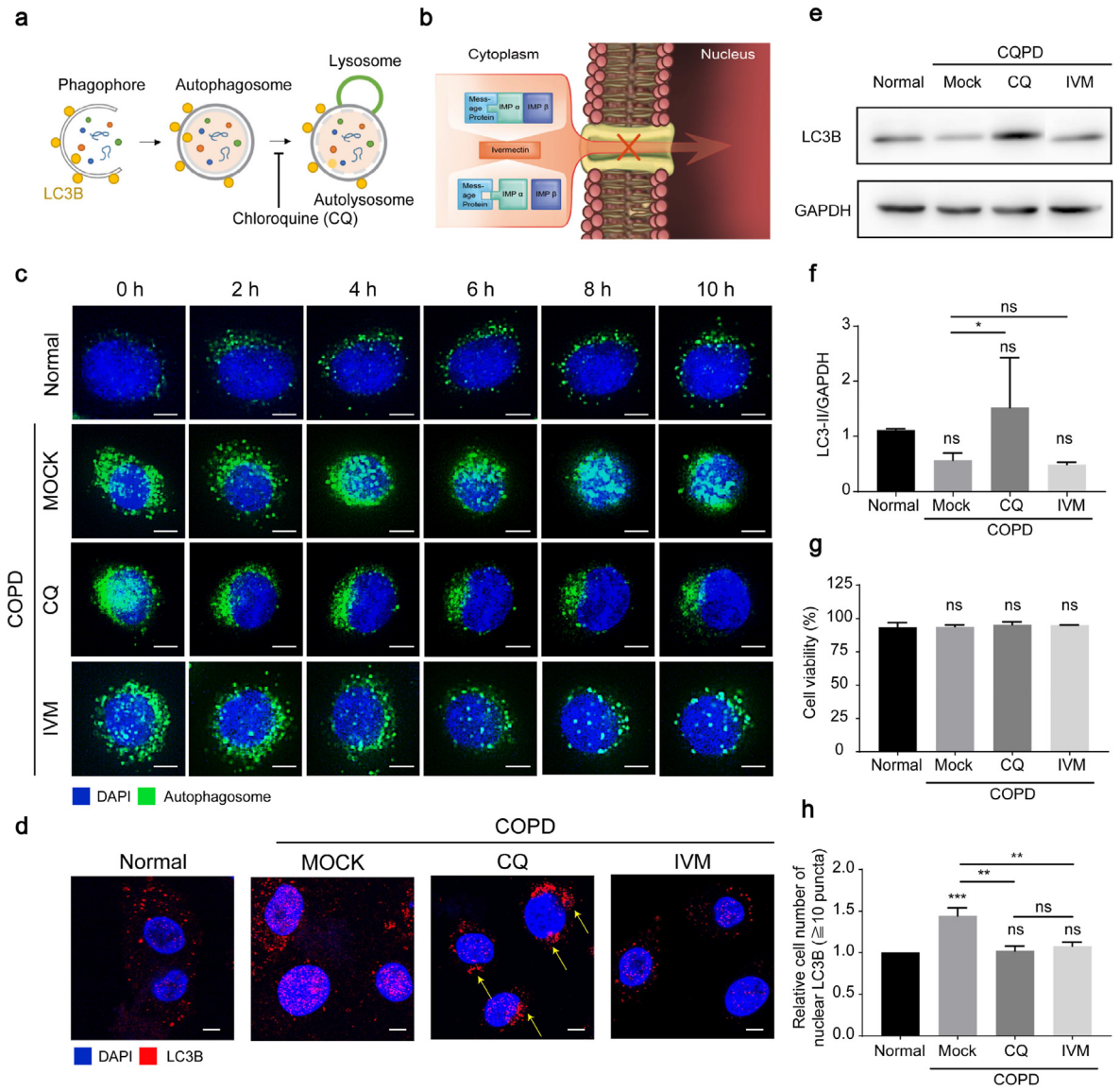

Fig. 2. CQ and IVM regulate LC3B expression of HSAECs. a, b) Schematic depicting the process and main regulatory mechanism of CQ and IVM. (a) Cells were treated with CQ to prevent binding of autophagosomes to lysosomes by changing the acidic environment of the lysosome. (b) IVM potently inhibits importin α/β (Impα/β1) nuclear import-dependent transport. c) High-content imaging system analysis of cells after CQ (10 μM) and IVM (200 μM) treatment, with live cell imaging of autophagy at 0, 2, 4, 6, 8, and 10 h. Cells were stained with DAPI (blue) and DAPGreen (green). d) LC3B expression in normal cells or COPD cells treated with or without CQ and IVM for 24 h. Cells were stained with DAPI (blue) and LC3B (red). (c), (d) Scale bar: 5 μm. e–f) Cells treated with CQ or IVM and LC3B levels were analyzed in the cytoplasm lysates. (e) Western blotting and (f) quantitative analysis of LC3B. g) Cell viability after treatment with CQ and IVM for 24 h. h) Relative LC3B puncta in the nucleus. Data were quantified using the high-content imaging system with at least 100 cells per condition from three independent experiments. ns: not significant. *P < 0.05, **P < 0.01, ***P < 0.001; values represent the mean ± SEM values (n = 3). (For interpretation of the references to colour in this figure legend, the reader is referred to the Web version of this article.)

differentiation were only 12% and 33% lower compared to normal cells, respectively (Fig. 3h and i). In contrast, the number of goblet cells after COPD cell differentiation was increased (Fig. 3j, Supplementary Fig. 3). Excessive airway mucus secretion is another important characteristic of chronic COPD and leads to inflammation, as well as potentially shortening the growth of cilia [28]. Our 3D images of differentiated cells showed that the cilia lengths were significantly shorter than those of cells obtained from the normal group (Fig. 3k). These results support that the characteristics and differences in the distribution of small airway tissue between normal and COPD cells can be reproduced in our optimized biomimetic differentiation model.

3.4. CQ and IVM respectively regulate the differentiation of cilia and mucus

As these two cell types exhibit differences in the expression of LC3B puncta in the nucleus, we next assessed whether this feature is an important mechanism for the differentiation and function of COPD cells (Fig. 4a). Fig. 4b shows that CQ specifically increased the efficiency of ciliated cells after differentiation. Interestingly, when COPD cells were stimulated with IVM, the differentiation effect of cilia was not significantly improved, but the differentiated goblet cells yielded the best performance (Fig. 4c). The confocal images revealed that after CQ stimulation, COPD cells tended to differentiate to in larger numbers and

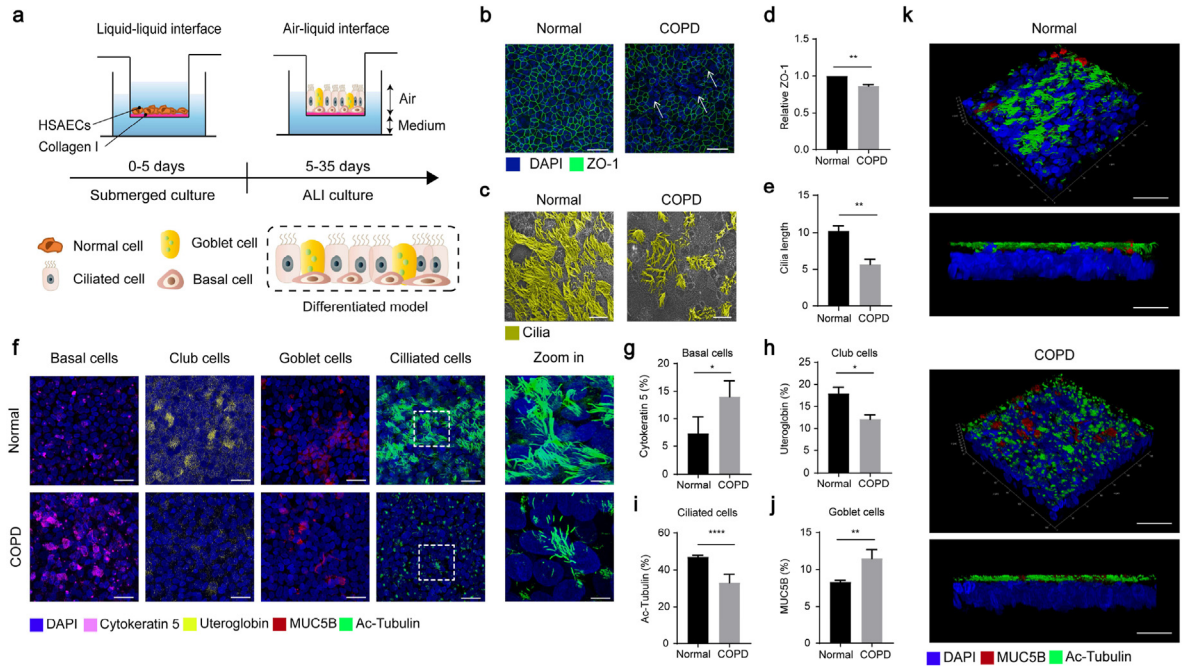

Fig. 3. Establishment and analysis of normal and COPD HSAEC differentiation model. a) Schematic of using the ALI culture method to establish a biomimetic airway differentiation model. b) Cells were stained with DAPI (blue) and ZO-1 (green). Scale bar: 50 μm. c) Scanning electron microscopy (SEM) of ciliated cells (yellow) on the surface of differentiated small airway epithelial. Scale bar: 10 μm. d) Quantitative analysis of ZO-1 expression. e) Quantification of ciliated cell length based on SEM images. The cilia lengths of normal cells were approximately 10 μm, and two-fold longer than those in COPD. f) Fluorescence staining and g–j) quantification of basal, club, ciliated, and goblet cells after differentiation (blue, DAPI; fuchsia, cytokeratin 5; yellow, uteroglobin; red, MUC5B; green, Ac-tubulin). Left scale bar: 25 μm, right scale bar: 5 μm. k) Three-dimensional (3D) confocal image of normal and COPD cells after differentiation. All fluorescence images were stained after ALI culture for 30 days. Scale bar: 25 μm*$P < 0.05$, **$P < 0.01$, ***$P < 0.001$, ****$P < 0.0001$; values represent the mean ± SEM values (n = 3). (For interpretation of the references to olor/colour in this figure legend, the reader is referred to the Web version of this article.)

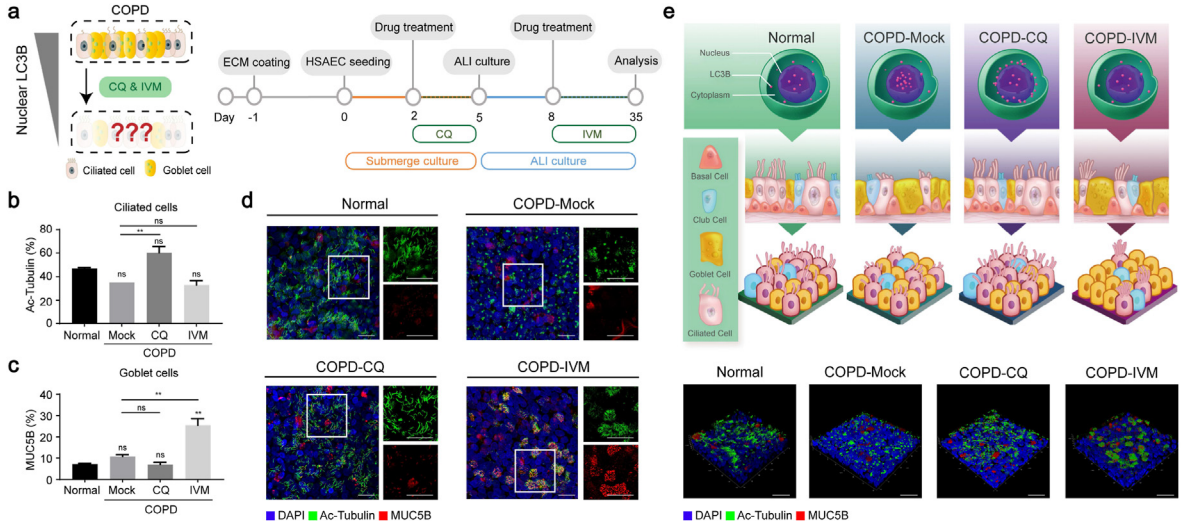

Fig. 4. Analysis of ciliated and goblet cells after CQ and IVM treatment of differentiated model. a) Timeline of HSAEC differentiation and CQ and IVM treatment. b, c) Quantitative analysis of ciliated and goblet cell expression in normal and COPD cells. d) Confocal images showing proportion of ciliated and goblet cells (blue, DAPI; green, Ac-tubulin; red, MUC5B). e) Schematic of ciliated and cell distribution and relative LC3B location after CQ and IVM regulation. ns: not significant. (d), (e) Scale bar: 25 μm**$P < 0.01$; Values represent the mean ± SEM values (n = 3). (For interpretation of the references to colour in this figure legend, the reader is referred to the Web version of this article.)

have longer cilia lengths, whereas after IVM stimulation, they differentiated into more mucus cells (Fig. 4d). Notably, differentiated cilia after IVM stimulation will have more significant characteristics of multiciliated cells [29,30]. Moreover, the red fluorescent signal of most goblet cells overlapped with that of ciliated cells, indicating that the differentiated cells were denser and clustered. These results show that in our biomimetic differentiation model, CQ and IVM regulated different aspects of LC3B in cells, thereby contributing to the differentiation of cilia and mucus (Fig. 4e).

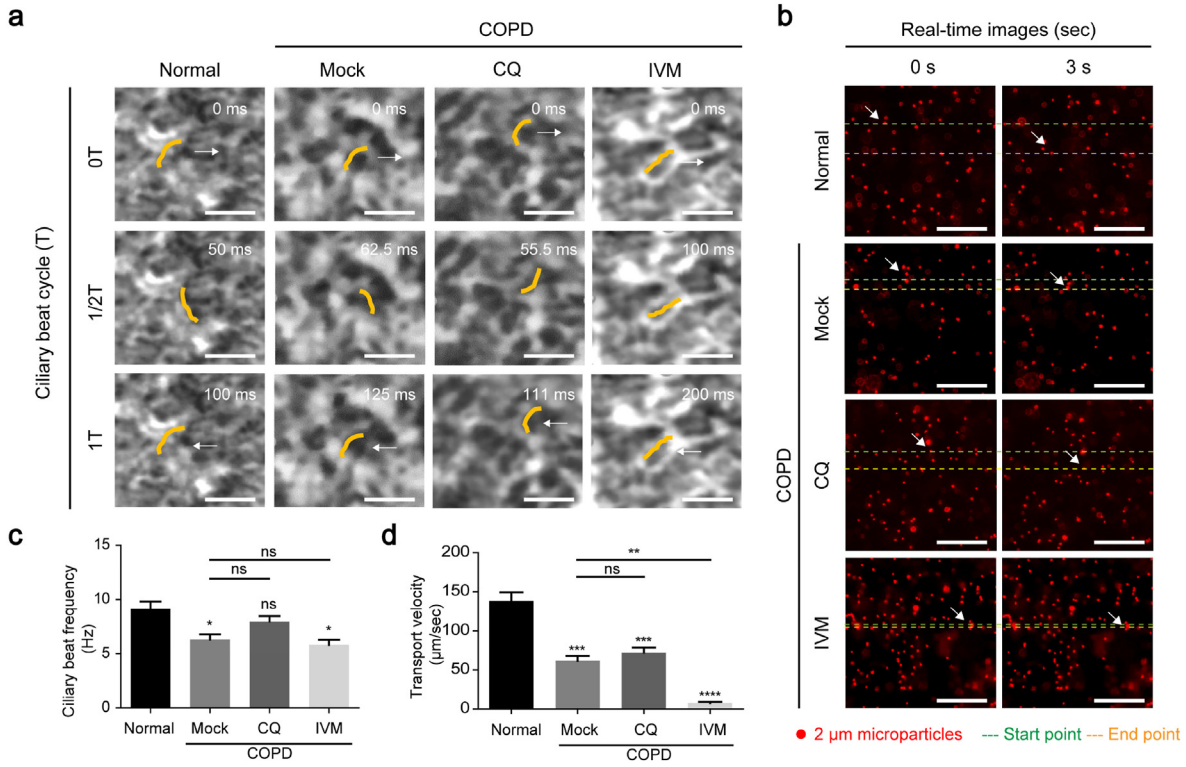

Fig. 5. Functional analysis of ciliated cells after CQ and IVM treatment. a) Sequential frames of a video of the surface of differentiated epithelium recording the time of one beating cycle (start: 0T, halfway: 1/2T, end: 1T. Individual cilia are highlighted in yellow in each frame; time stamps and the white arrow indicate the duration and direction of one forward and return stroke (Supplementary Videos 1–4 show the full recording). Scale bar: 10 μm. b) Transport velocity was evaluated by adding 2 μm red fluorescent microspheres to the differentiated cilia, and the moving distance was measured within 3 s. Scale bar: 100 μm. c) Cilia beat frequency = 1/T. d) Transport velocity was calculated using 2-μm red fluorescent microspheres in real-time video. ns: not significant. $^{**}P < 0.01$; values represent the mean ± SEM values. Four different groups (healthy, COPD, COPD + CQ, COPD + IVM) were evaluated in 3 independent experiments on different transwells. In each group, ImageJ software was used to analyze the duration of one beating cycle for more than 10,000 cilia and to track the trajectory and movement rate of more than 500 nanoparticles. (For interpretation of the references to colour in this figure legend, the reader is referred to the Web version of this article.)

3.5. CQ regulation of cilia function

To clarify the influence of CQ and IVM on ciliary function, we analyzed the oscillation frequency of cilia. The time required for the differentiated cilia to beat once in the COPD group was approximately 125 ms, which is longer than the 100 ms in the normal group (Fig. 5a). However, after stimulating the COPD cells with CQ, cilia differentiation was improved and the oscillation frequency was effectively recovered. In contrast, COPD cells stimulated with IVM showed no significant improvement, and the time required for one beat increased to approximately 200 ms. To confirm this result, we used red fluorescent-labeled microspheres (sizes = 2 μm) to determine the ability of cilia to remove particles after differentiation. As shown in Fig. 5b, in addition to the slower oscillation frequency of the differentiated cilia from COPD cells, the ability to remove particles was also significantly reduced compared to in the normal group. The cilia cells that differentiated after stimulation with CQ and IVM showed the same tendency as the oscillation frequency in their ability to remove particles (Fig. 5c and d). Excessive mucus production caused by IVM stimulation may have been the main reason for the limited ability of cilia to beat and remove particles. Because of the differences between CQ and IVM in recovering cilia, our results show that even after treatment with different LC3B mechanism inhibitors, corresponding and reliable airway differentiation and functional differences were observed in our biomimetic differentiation model.

4. Discussion

Although numerous studies have focused on autophagy in the pathogenic mechanisms of COPD, most studies only focused on common autophagic reactions and mechanisms [31–34]. Based on recent progress in understanding the autophagic mechanisms [35–38], the regulation of LC3B in the nucleus has been shown to be related to many diseases and physiological functions [39–42] but the underlying mechanisms are poorly understood in lung-related diseases or small airway epithelial cells. Previously, only different types of cells in small airways were shown to exhibit different degrees of autophagy [43]. Among them, ciliated cells showed the highest expressions of LC3B amongst basal and goblet cells. Therefore, regulating the autophagic response mainly affects the function of cilia. We found that HSAECs of COPD had a different autophagic response compared with that of normal cells. Although the detailed mechanism of cell differentiation remains unclear, compared to the previous autophagy regulation, our results suggest that cell differentiation occurs through regulation of LC3B in cells.

To validate these results, we tested another common inhibitor of autophagy, 3-MA, which can prevent autophagosome formation by inhibiting phosphatidyl-inositol 3-kinase [44]. When COPD cells were treated with 3-MA for 4 h, the expression of LC3B in the cytoplasm and nucleus continued to decrease (Supplementary Fig. 4a–c). These data revealed that 3-MA did not increase the differentiation efficiency of ciliated and goblet cells and led to a shorter cilia length compared to cells in the normal group (Supplementary Fig. 4d). These results reveal that although the regulation autophagy mechanism can increase the differentiation efficiency of HSAECs, excessive inhibition leads to the loss of cell differentiation. It is necessary to regulate the expression and distribution of LC3B in the nucleus and cytoplasm, which is key to HSAEC differentiation.

Notably, compared with traditional cell culture and differentiation methods [45–47], by adjusting the collagen coating, cell density, culture

medium composition, and the time point of transition from submerged to ALI culture, small airway differentiation can be effectively induced without additional cell mechanical stress [48–50] and maintain a physiological microenvironment similar to that in the human body and recapitulate functionally differentiated cell types, including basal, secretory, mucous, and ciliated cells. The length and beating of cilia also yielded data similar to those in the human body (Supplementary Table S3), verifying that the biomimetic model of small airways can provide a better representation of physiological data.

Using our biomimetic differentiation model, we showed that CQ stimulation can improve the cilia function of COPD cells, with the beating frequency similar to that of normal cilia. However, despite exhibiting the differentiation characteristics of multi-ciliated cells, the beating frequency and efficiency for removing particles remained limited following stimulation with IVM. When motile cilia were enriched, mucus accumulation between the cilia may not have been eliminated in nondynamic culture. Although we combined IVM with *S*-(carboxymethyl)-L-cysteine and guaiacol glycerol ether to remove the mucus [51,52], there was no significant increase in the frequency of cilia beating (Supplementary Fig. 5). A more dynamic biomimetic system developed in recent years can also be considered [53,54]. Compared with the results from animal experiments, the use of such a biomimetic system can yield physiological and inflammatory responses that closely match those in the clinical setting and accelerate the identification of specific biomarkers for further analysis [55–58].

Here, we successfully explored the LC3B mechanism and influence of cell differentiation using an optimized *in vitro* model. The cells used in the defined models are commercial stable normal and COPD cells. However, cells from different clinical sources or individuals, such as from people of different sexes or ages, may lead to more diverse experimental results regarding the biological responses. For example, autophagy shows sex differences between cells, cell differentiation, and even airway disease characteristics [59–61]. Studies also have proposed that autophagy is a survival mechanism in males, and autophagy in females leads to cell death derived from separation [62]. Sex differences in innate autophagy have also been observed in rats, and this sex dimorphism is organ-specific [63]. Therefore, regardless of sex, age, and other individual differences, the impact of the LC3B mechanism on cell differentiation should be further investigated.

Furthermore, our results show that normal cells exhibit increased accumulation of LC3B in the nucleus after stimulation by LPS; thus, this biological response may not be specific to COPD, and even under different stages of COPD, cells may show slight changes in autophagy markers or subsequent cilia differentiation. In addition, such biological responses in normal cells may vary in degree because of smoking or cilia expression. For example, increased ACE2 expression has been observed in small airway epithelium samples of healthy smokers compared to in nonsmokers [64]. Another recent study indicated that ACE2 is abundant in ciliated cells of the respiratory tract but not in goblet cells [65]. Based on our biomimetic model, ACE2 was indeed expressed in large amounts in ciliated cells (Supplementary Fig. 6). Interestingly, LC3B is also expressed in large amounts in ciliated cells but is not expressed in goblet cells [66,67], showing similar performance characteristics as ACE2. The interaction between LC3B and ACE2, as well as the influence of smoking on these physiological mechanisms and subsequent ciliary differentiation, should be further examined.

In summary, we determined the differential expression and characteristics of autophagic protein LC3B in the nucleus of normal and COPD HSAECs and optimized the small airway *in vitro* ALI differentiation model and 3D image reconstruction features. Our further studies will focus on the differentiation of cilia and mucus in this unique physiological mechanism, as well as subsequent cilia function. We explored the cilia differentiation and function of small airway epithelial cells and investigated LC3B expression following treatments with the inhibitors CQ and IVM. The improved differentiation and function of cilia overcome the limitations of previous *in vitro* experiments; our model is useful for exploring the biological mechanism of COPD and cell differentiation strategies.

Credit author statement

Shiue-Luen Chen: Conceptualization, Investigation, Methodology, Project administration, Writing – original draft. **Hsiao-Chun Chou:** Conceptualization, Investigation, Methodology, Project administration, Writing – original draft. **Kuan-Chen Lin:** Data curation, Methodology, Investigation, Writing – original draft. **Jia-Wei Yang:** Writing – review & editing. **Ren-Hao Xie:** Data curation, Methodology, Software. **Chong-You Chen:** Data curation, Methodology, Software. **Xin-Yi Liu:** Data curation, Methodology, Software. **Johnson H.Y Chung:** Writing – review & editing. **Guan-Yu Chen:** Project administration, Funding acquisition, Supervision, Writing – review & editing.

Declaration of competing interest

The authors declare that they have no known competing financial interests or personal relationships that could have appeared to influence the work reported in this paper.

Acknowledgements

G.Y.C. would like to acknowledge financial support from the Ministry of Science and Technology (MOST-110-2636-E-009-007-, MOST-111-2636-E-009-005-), National Health Research Institutes (NHRI-EX110-10714EC), Council of Agriculture, Executive Yuan (110AS-24.2.1-AD-U2, 111AS-13.2.1-AD-U2) and the Higher Education Sprout Project of the National Yang Ming Chiao Tung University and the Ministry of Education, Taiwan.

Appendix A. Supplementary data

Supplementary data to this article can be found online at https://doi.org/10.1016/j.mtbio.2021.100182.

References

[1] A. Agustí, J.C. Hogg, Update on the pathogenesis of chronic obstructive pulmonary disease, N. Engl. J. Med. 381 (13) (2019) 1248–1256.
[2] B.R. Celli, J.A. Wedzicha, Update on clinical aspects of chronic obstructive pulmonary disease, N. Engl. J. Med. 381 (13) (2019) 1257–1266.
[3] G.A. Roth, D. Abate, K.H. Abate, S.M. Abay, C. Abbafati, N. Abbasi, et al., Global, regional, and national age-sex-specific mortality for 282 causes of death in 195 countries and territories, 1980–2017: a systematic analysis for the Global Burden of Disease Study 2017, Lancet 392 (10159) (2018) 1736–1788.
[4] J.A. Aguiar, A. Tamminga, B. Lobb, R.D. Huff, J.P. Nguyen, Y. Kim, et al., The impact of cigarette smoke exposure, COPD, or asthma status on ABC transporter gene expression in human airway epithelial cells, Sci. Rep. 9 (1) (2019) 1–12.
[5] P.C. Veerati, N.M. Troy, A.T. Reid, N.F. Li, K.S. Nichol, P. Kaur, et al., Airway epithelial cell immunity is delayed during rhinovirus infection in asthma and COPD, Front. Immunol. 11 (2020) 974.
[6] N. Nachmias, S. Langier, R.Y. Brzezinski, M. Siterman, M. Stark, S. Etkin, et al., NLRP3 inflammasome activity is upregulated in an in-vitro model of COPD exacerbation, PLoS One 14 (5) (2019), e0214622.
[7] M. Bodas, G. Pehote, D. Silverberg, E. Gulbins, N. Vij, Autophagy augmentation alleviates cigarette smoke-induced CFTR-dysfunction, ceramide-accumulation and COPD-emphysema pathogenesis, Free Radic. Biol. Med. 131 (2019) 81–97.
[8] Y.-F. Wu, Z.-Y. Li, L.-L. Dong, W.-J. Li, Y.-P. Wu, J. Wang, et al., Inactivation of MTOR promotes autophagy-mediated epithelial injury in particulate matter-induced airway inflammation, Autophagy 16 (3) (2020) 435–450.
[9] X. Lv, K. Li, Z. Hu, Chronic Obstructive Pulmonary Disease and Autophagy. Autophagy: Biology and Diseases, Springer, 2020, pp. 559–567.
[10] K.D. McAlinden, D.A. Deshpande, S. Ghavami, D. Xenaki, S.S. Sohal, B.G. Oliver, et al., Autophagy activation in asthma airways remodeling, Am. J. Respir. Cell Mol. Biol. 60 (5) (2019) 541–553.
[11] K. Arora, J.R. Lund, N.A. Naren, B. Zingarelli, A.P. Naren, AC6 regulates the microtubule-depolymerizing kinesin KIF19A to control ciliary length in mammals, J. Biol. Chem. 295 (42) (2020) 14250–14259.
[12] A.H. Lystad, S.R. Carlsson, R. Laura, K.J. Kauffman, S. Nag, T. Yoshimori, et al., Distinct functions of ATG16L1 isoforms in membrane binding and LC3B lipidation in autophagy-related processes, Nat. Cell Biol. 21 (3) (2019) 372–383.

[13] M.W. Baeken, K. Weckmann, P. Diefenthäler, J. Schulte, K. Yusifli, B. Moosmann, et al., Novel insights into the cellular localization and regulation of the autophagosomal proteins LC3A, LC3B and LC3C, Cells 9 (10) (2020) 2315.
[14] O. Pampliega, I. Orhon, B. Patel, S. Sridhar, A. Díaz-Carretero, I. Beau, et al., Functional interaction between autophagy and ciliogenesis, Nature 502 (7470) (2013) 194–200.
[15] V. Gies, N. Bekaddour, Y. Dieudonné, A. Guffroy, Q. Frenger, F. Gros, et al., Beyond anti-viral effects of chloroquine/hydroxychloroquine, Front. Immunol. 11 (2020) 1409.
[16] M. Mauthe, I. Orhon, C. Rocchi, X. Zhou, M. Luhr, K.-J. Hijlkema, et al., Chloroquine inhibits autophagic flux by decreasing autophagosome-lysosome fusion, Autophagy 14 (8) (2018) 1435–1455.
[17] M.I. Koukourakis, D. Kalamida, A. Giatromanolaki, C.E. Zois, E. Sivridis, S. Pouliliou, et al., Autophagosome proteins LC3A, LC3B and LC3C have distinct subcellular distribution kinetics and expression in cancer cell lines, PLoS One 10 (9) (2015), e0137675.
[18] L. Caly, J.D. Druce, M.G. Catton, D.A. Jans, K.M. Wagstaff, The FDA-approved drug ivermectin inhibits the replication of SARS-CoV-2 in vitro, Antivir. Res. 178 (2020) 104787.
[19] G.Y. Chen, D.W. Pang, S.M. Hwang, H.Y. Tuan, Y.C. Hu, A graphene-based platform for induced pluripotent stem cells culture and differentiation, Biomaterials 33 (2) (2012) 418–427.
[20] W.S.D. Tan, H.M. Shen, W.S.F. Wong, Dysregulated autophagy in COPD: a pathogenic process to be deciphered, Pharmacol. Res. 144 (2019) 1–7.
[21] S.W. Ryter, A.M. Choi, Autophagy in lung disease pathogenesis and therapeutics, Redox. Biol. 4 (2015) 215–225.
[22] Z.H. Chen, H.P. Kim, F.C. Sciurba, S.J. Lee, C. Feghali-Bostwick, D.B. Stolz, et al., Egr-1 regulates autophagy in cigarette smoke-induced chronic obstructive pulmonary disease, PLoS One 3 (10) (2008), e3316.
[23] K. Matter, S. Aijaz, A. Tsapara, M.S. Balda, Mammalian tight junctions in the regulation of epithelial differentiation and proliferation, Curr. Opin. Cell Biol. 17 (5) (2005) 453–458.
[24] U. Kyung, S.D.R. Hong, Watkins Simon, Fuchs Elaine, Barry R. Stripp, Basal cells are a multipotent progenitor capable of renewing the bronchial epithelium, Pathology 164 (2004).
[25] R. Shaykhiev, R.G. Crystal, Early events in the pathogenesis of chronic obstructive pulmonary disease. Smoking-induced reprogramming of airway epithelial basal progenitor cells, Ann. Am. Thorac. Soc. 11 (Suppl 5) (2014) S252–S258.
[26] M.R. Staudt, L.J. Buro-Auriemma, M.S. Walters, J. Salit, T. Vincent, R. Shaykhiev, et al., Airway Basal stem/progenitor cells have diminished capacity to regenerate airway epithelium in chronic obstructive pulmonary disease, Am. J. Respir. Crit. Care Med. 190 (8) (2014) 955–958.
[27] W. Rokicki, M. Rokicki, J. Wojtacha, A. Dzeljijli, The role and importance of club cells (Clara cells) in the pathogenesis of some respiratory diseases, Kardiochir Torakochirurgia Pol 13 (1) (2016) 26–30.
[28] Y. Shen, S. Huang, J. Kang, J. Lin, K. Lai, Y. Sun, et al., Management of airway mucus hypersecretion in chronic airway inflammatory disease: Chinese expert consensus (English edition), Int. J. Chronic Obstr. Pulm. Dis. 13 (2018) 399–407.
[29] R. Nanjundappa, D. Kong, K. Shim, T. Stearns, S.L. Brody, J. Loncarek, et al., Regulation of cilia abundance in multiciliated cells, Elife 8 (2019), e44039.
[30] O. Mercey, M.S. Levine, G.M. LoMastro, P. Rostaing, E. Brotslaw, V. Gomez, et al., Massive centriole production can occur in the absence of deuterosomes in multiciliated cells, Nat. Cell Biol. 21 (12) (2019) 1544–1552.
[31] K. Mizumura, S. Maruoka, T. Shimizu, Y. Gon, Autophagy, selective autophagy, and necroptosis in COPD, Int. J. Chronic Obstr. Pulm. Dis. 13 (2018) 3165–3172.
[32] K. Mizumura, S. Cloonan, M.E. Choi, S. Hashimoto, K. Nakahira, S.W. Ryter, et al., Autophagy: friend or foe in lung disease? Ann. Am. Thorac. Soc. 13 (Suppl 1) (2016) S40–S47. Suppl 1.
[33] N. Vij, P. Chandramani-Shivalingappa, C. Van Westphal, R. Hole, M. Bodas, Cigarette smoke-induced autophagy impairment accelerates lung aging, COPD-emphysema exacerbations and pathogenesis, Am. J. Physiol. Cell Physiol. 314 (1) (2018) C73–c87.
[34] A.C. Racanelli, S.A. Kikkers, A.M.K. Choi, S.M. Cloonan, Autophagy and inflammation in chronic respiratory disease, Autophagy 14 (2) (2018) 221–232.
[35] T. Johansen, T. Lamark, Selective autophagy: ATG8 family proteins, LIR Motifs and cargo receptors, J. Mol. Biol. 432 (1) (2020) 80–103.
[36] M. Yoshida, S. Minagawa, J. Araya, T. Sakamoto, H. Hara, K. Tsubouchi, et al., Involvement of cigarette smoke-induced epithelial cell ferroptosis in COPD pathogenesis, Nat. Commun. 10 (1) (2019) 3145.
[37] M. Allegretti, C.E. Zimmerli, V. Rantos, F. Wilfling, P. Ronchi, H.K.H. Fung, et al., In-cell architecture of the nuclear pore and snapshots of its turnover, Nature 586 (7831) (2020) 796–800.
[38] I. Serramito-Gómez, E. Boada-Romero, R. Villamuera, Á. Fernández-Cabrera, J.L. Cedillo, Á. Martín-Regalado, et al., Regulation of cytokine signaling through direct interaction between cytokine receptors and the ATG16L1 WD40 domain, Nat. Commun. 11 (1) (2020) 5919.
[39] R. Huang, Y. Xu, W. Wan, X. Shou, J. Qian, Z. You, et al., Deacetylation of nuclear LC3 drives autophagy initiation under starvation, Mol. Cell 57 (3) (2015) 456–466.
[40] R. Huang, W. Liu, Identifying an essential role of nuclear LC3 for autophagy, Autophagy 11 (5) (2015) 852–853.
[41] M.E. Papandreou, N. Tavernarakis, Nucleophagy: from homeostasis to disease, Cell Death Differ. 26 (4) (2019) 630–639.
[42] M.S. Shim, A. Nettesheim, J. Hirt, P.B. Liton, The autophagic protein LC3 translocates to the nucleus and localizes in the nucleolus associated to NUFIP1 in response to cyclic mechanical stress, Autophagy 16 (7) (2020) 1248–1261.
[43] D. Pham, G.Y. Ban, S.H. Kim, Y. Shin, Y.M. Ye, Y.J. Chwae, et al., Neutrophil autophagy and extracellular DNA traps contribute to airway inflammation in severe asthma, Clin. Exp. Allergy 47 (1) (2017) 57–70.
[44] X. Jiang, L. Fang, H. Wu, X. Mei, F. He, P. Ding, et al., TLR2 regulates allergic airway inflammation and autophagy through PI3K/Akt signaling pathway, Inflammation 40 (4) (2017) 1382–1392.
[45] A. Artzy-Schnirman, S.A. Raviv, O.D. Flikshtain, J. Shklover, N. Korin, A. Gross, et al., Advanced human-relevant in vitro pulmonary platforms for respiratory therapeutics, Adv. Drug Deliv. Rev. (2021) 113901.
[46] A. Artzy-Schnirman, C.-M. Lehr, J. Sznitman, Advancing human in vitro pulmonary disease models in preclinical research: opportunities for lung-on-chips, Expet Opin. Drug Deliv. 17 (5) (2020) 621–625.
[47] M. Sakagami, In vitro, ex vivo and in vivo methods of lung absorption for inhaled drugs, Adv. Drug Deliv. Rev. 161-162 (2020) 63–74.
[48] P. Zamprogno, S. Wüthrich, S. Achenbach, G. Thoma, J.D. Stucki, N. Hobi, et al., Second-generation lung-on-a-chip with an array of stretchable alveoli made with a biological membrane, Communication. Biol. 4 (1) (2021) 168.
[49] A. Doryab, M.B. Taskin, P. Stahlhut, A. Schröppel, S. Orak, C. Voss, et al., A bioinspired in vitro lung model to study particokinetics of nano-/microparticles under cyclic stretch and air-liquid interface conditions, Front. Bioeng. Biotechnol. 9 (2021) 616830.
[50] M. Felder, B. Trueeb, A.O. Stucki, S. Borcard, J.D. Stucki, B. Schnyder, et al., Impaired wound healing of alveolar lung epithelial cells in a breathing lung-on-A-chip, Front. Bioeng. Biotechnol. 7 (2019) 3.
[51] X. Li, F. Jin, H.J. Lee, C.J. Lee, Recent advances in the development of novel drug candidates for regulating the secretion of pulmonary mucus, Biomolecules therapeutics 28 (4) (2020) 293.
[52] V. Dinu, A. Kilic, Q. Wang, C. Ayed, A. Fadel, S.E. Harding, et al., Policy, toxicology and physicochemical considerations on the inhalation of high concentrations of food flavour, NPJ Sci. Food 4 (1) (2020) 1–10.
[53] K.H. Benam, M. Mazur, Y. Choe, T.C. Ferrante, R. Novak, D.E. Ingber, Human lung small airway-on-a-chip protocol, Methods Mol. Biol. 1612 (2017) 345–365.
[54] K.H. Benam, R. Villenave, C. Lucchesi, A. Varone, C. Hubeau, H.H. Lee, et al., Small airway-on-a-chip enables analysis of human lung inflammation and drug responses in vitro, Nat. Methods 13 (2) (2016) 151–157.
[55] K.H. Benam, M. Mazur, Y. Choe, T.C. Ferrante, R. Novak, D.E. Ingber, Human Lung Small Airway-On-A-Chip Protocol. 3D Cell Culture, Springer, 2017, pp. 345–365.
[56] M. Humayun, C.-W. Chow, E.W. Young, Microfluidic lung airway-on-a-chip with arrayable suspended gels for studying epithelial and smooth muscle cell interactions, Lab Chip 18 (9) (2018) 1298–1309.
[57] B.A. Hassell, G. Goyal, E. Lee, A. Sontheimer-Phelps, O. Levy, C.S. Chen, et al., Human organ chip models recapitulate orthotopic lung cancer growth, therapeutic responses, and tumor dormancy in vitro, Cell Rep. 21 (2) (2017) 508–516.
[58] J. Shrestha, S. Razavi Bazaz, H. Aboulkheyr Es, D. Yaghobian Azari, B. Thierry, M. Ebrahimi Warkiani, et al., Lung-on-a-chip: the future of respiratory disease models and pharmacological studies, Crit. Rev. Biotechnol. 40 (2) (2020) 213–230.
[59] P.B. Dominelli, J.G. Ripoll, T.J. Cross, S.E. Baker, C.C. Wiggins, B.T. Welch, et al., Sex differences in large conducting airway anatomy, J. Appl. Physiol. 125 (3) (2018) 960–965.
[60] D. Raghavan, R. Jain, Increasing awareness of sex differences in airway diseases, Respirology 21 (3) (2016) 449–459.
[61] N.S. Ambhore, R.S.R. Kalidhindi, V. Sathish, Sex-steroid signaling in lung diseases and inflammation, Adv. Exp. Med. Biol. 1303 (2021) 243–273.
[62] I. Vega-Naredo, B. Caballero, V. Sierra, C. Huidobro-Fernández, D. de Gonzalo-Calvo, M. García-Macia, et al., Sexual dimorphism of autophagy in Syrian hamster Harderian gland culminates in a holocrine secretion in female glands, Autophagy 5 (7) (2009) 1004–1017.
[63] I. Campesi, E. Straface, S. Occhioni, A. Montella, F. Franconi, Protein oxidation seems to be linked to constitutive autophagy: a sex study, Life Sci. 93 (4) (2013) 145–152.
[64] J. Alderden, L.J. Cowan, J.B. Dimas, D. Chen, Y. Zhang, M. Cummins, et al., Risk factors for hospital-acquired pressure injury in surgical critical care patients, Am. J. Crit. Care : Off. Pub. Am. Assoc. Critical Care Nurses 29 (6) (2020) e128–e134.
[65] I.T. Lee, T. Nakayama, C.T. Wu, Y. Goltsev, S. Jiang, P.A. Gall, et al., ACE2 localizes to the respiratory cilia and is not increased by ACE inhibitors or ARBs, Nat. Commun. 11 (1) (2020) 5453.
[66] M. Qi, J. Zhou, X. Zhang, X. Zhong, Y. Zhang, X. Zhang, et al., Effect of Xiaoqinglong decoction on mucus hypersecretion in the airways and cilia function in a murine model of asthma, J. Traditional Chinese Sci. 4 (3) (2017) 290–296.
[67] J.-E. Bae, G.M. Kang, S.H. Min, D.S. Jo, Y.-K. Jung, K. Kim, et al., Primary cilia mediate mitochondrial stress responses to promote dopamine neuron survival in a Parkinson's disease model, Cell Death Dis. 10 (12) (2019) 1–15.